Journal of Water & Health

Journal of Water and Health Vol 20 No 12, 1673 doi: 10.2166/wh.2022.293

A glass matrices-assisted quantum dots-based biosensor for selective capturing and detection of *Escherichia coli*

Anjali Pant[a], Taranvir Kaur[a], Teenu Sharma[b], Joga Singh[a], Ashish Suttee[c], Ravi Pratap Barnwal[d], Indu Pal Kaur[a], Gurpal Singh[a,*] and Bhupinder Singh [a,b]

[a] University Institute of Pharmaceutical Sciences, Panjab University, Chandigarh, India 160014
[b] Chitkara College of Pharmacy, Chitkara University, Rajpura, Punjab, India 140401
[c] Department of Pharmacognosy, School of Pharmaceutical Sciences, Lovely Professional University, Jalandhar, Punjab, India
[d] Department of Biophysics, Panjab University, Chandigarh, India 160014
*Corresponding author. E-mail: gurpalsingh.ips@gmail.com

BS, 0000-0001-5205-6258

ABSTRACT

Bacterial contamination of water and food is a grave health concern rendering humans quite vulnerable to disease(s), and proving, at times, fatal too. Exploration of the novel diagnostic tools is, accordingly, highly called for to ensure rapid detection of the pathogenic bacteria, particularly *Escherichia coli*. The current manuscript, accordingly, reports the use of silane-functionalized glass matrices and antibody-conjugated cadmium telluride (CdTe) quantum dots (QDs) for efficient detection of *E. coli*. Synthesis of QDs (size: 5.4–6.8 nm) using mercaptopropionic acid (MPA) stabilizer yielded stable photoluminescence (~62%), corroborating superior fluorescent characteristics. A test sample, when added to antibody-conjugated matrices, followed by antibody-conjugated CdTe-MPA QDs, formed a pathogen-antibody QDs complex. The latter, during confocal microscopy, demonstrated rapid detection of the selectively captured pathogenic bacteria (10 microorganism cells/10 μL) with enhanced sensitivity and specificity. The work, overall, encompasses establishment and design of an innovative detection platform in microbial diagnostics for rapid capturing of pathogens in water and food samples.

Key words: antibody, bacteria, microbial detection, pathogenic contamination, quantum dots, water sample

HIGHLIGHTS

- Antibody-mediated fluorescent biosensor for efficient capturing and detection of *E. coli*.
- Bioconjugation of QDs and *E. coli* antibodies.
- Qualitative, quantitative and selective assessment of *E. coli* in contaminated water using CLSM.
- High sensitivity of glass matrix biosensor, with detection limit of 10 microorganisms/10 mL.
- Capability of technology extension for detecting other microbial pathogens.

GRAPHICAL ABSTRACT

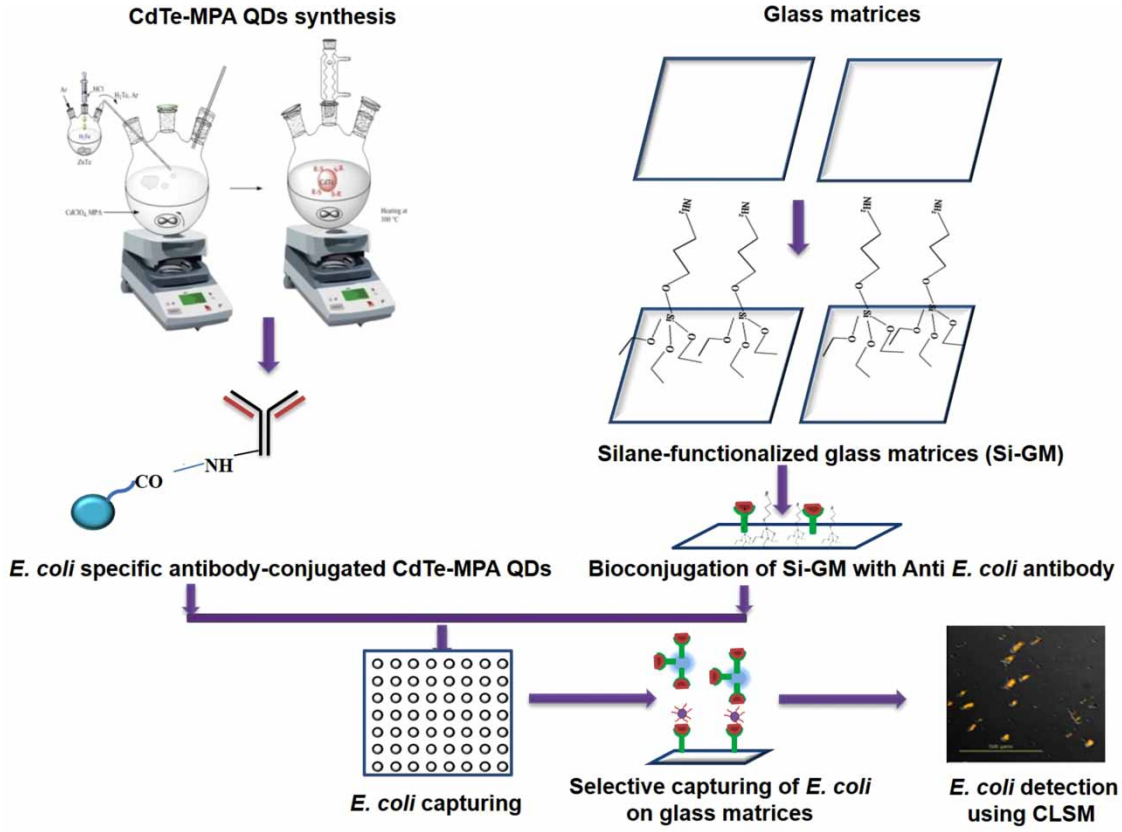

1. INTRODUCTION

Hygienic food and water are the primary requirements for human survival. Nearly 60% of annual deaths are reported to occur owing to water-borne diseases alone (Lee *et al.* 2018). Biological pathogens, as plausible contaminants in water, constitute one of the major factors accounting for mortality among humans, the presence of which in potable water has been attributed to lack of sewage management and apt sanitation facilities (Alahi & Mukhopadhyay 2017). The primary bacterial pathogens, in this regard, encompass *Escherichia coli*, *Leptospira interrogans*, *Salmonella enterica*, *Campylobacter jejuni*, *Staphylococcus aureus*, *Clostridium difficile*, *Listeria monocytogenes*, *Bacillus cereus* and *Vibrio cholera* (Bhardwaj *et al.* 2019). Among these, *E. coli*, a Gram-negative bacterium, is abundantly found in the lower intestine of humans. Strains of *E. coli* are invariably pathogenic, causing gastro-intestinal diseases, urinary tract infections and even bacterial meningitis in the neonates. Being considered as a zero-tolerance pathogen, there is an ardent need for novel and efficient approaches for rapid diagnosis, and subsequent prevention and therapeutic management of *E. coli* infections. Traditional approaches employed in recent years, such as culturing of bacteria on agar plates followed by standard biochemical identifications (Law *et al.* 2015), ELISA test involving multiple washing steps (Pang *et al.* 2018; Wu *et al.* 2019), flow cytometry, 24-h pre-treatment procedure in lateral flow assay (Luo *et al.* 2020), polymerase chain reaction, immune-magnetic separation and bacteria-specific aptamers with microchip capillary electrophoresis-coupled laser-induced fluorescence (Zhang *et al.* 2019) have resulted in different degrees of fruition, but were found to quite time-consuming, more laborious, less sensitive, expensive and requiring skilled technical manpower (Bursle & Robson 2016). Nanotechnology has provided considerable opportunities to address these problems by closely integrating diagnosis with therapeutic management of various ailments. Nanoparticle (NP)-based molecular imaging and therapy, therefore, have been successfully explored as a powerful model for non-invasive disease diagnosis (Liu *et al.* 2007; Nie *et al.* 2007).

The use of quantum dots (QDs) in biosensor diagnostic devices has undertaken for designing various devices to produce signals proportional to the concentration of the desired analyte and serve as an efficient detection tool (Mansuriya & Altintas

2020; Li *et al.* 2021). These are the semiconducting nanocrystals or NPs that demonstrate properties ranging between those of discrete molecules and bulk semiconductors (Grabolle *et al.* 2009; Kuzyniak *et al.* 2014). QDs offer stellar advantages over the fluorescent dyes, like intense and stable fluorescence for longer times, and resistance to photo-bleaching. Because of their minuscule size, high surface-to-volume ratio and high sensitivity, these QDs have proved to be efficient detection tools (Acharya *et al.* 2017; Bedi *et al.* 2022; Pandit *et al.* 2022; Petronella *et al.* 2022). Some recent studies have been reported, employing antibody QDs for successful detection of the pathogens in various foods (Du *et al.* 2021).

The present research work, therefore, endeavors to explore a novel, cost-effective, quick, specific and sensitive technique for detecting the presence of the pathogens in water samples. The work focuses on the development of bioconjugated cadmium-based QDs with significant fluorescent properties for efficient detection of pathogenic bacterium, i.e., *E. coli* ATCC 25922, adopting a sandwich technique employing antibody-conjugated QDs on layers of bacteria, immobilized with silane-functionalized glass matrices. The novelty of our work is to develop a glass matrices-based biosensor employing the use of antibodies as a biorecognition target which will be able to capture the pathogenic bacteria in aqueous sample and in turn produce a transducing signal in lieu of fluorescence produced by the cadmium-based QDs. A provisional patent on the current work, successfully filed by us in 2019, has very recently been published too. Subsequently, taking ostensible leads from our patent (Singh *et al.* 2020), another study, employing such as sandwich technique and cadmium-based QDs, has recently been reported (Ravikumar *et al.* 2020). Accordingly, the authors herein report the explicit details of our research work, carried out in a systematic manner.

2. MATERIALS AND METHODS

2.1. Materials

Cadmium perchlorate (Sigma-Aldrich, St. Louis, MO, USA), 1-(3-dimethylaminopropyl)-3-ethylcarbodiimidehydrochloride (EDC) (TCI, Tokyo, Japan), 1-octadecene, (3-aminopropyl) triethoxysilane, (3-aminopropyl) triethoxysilane (APTES) and 3-mercaptopropionic acid (3-MPA) were purchased from M/s Alfa Aesar, Heysham, England, 1,2-dichlorobenzene (Loba-Chemie, Pvt. Ltd Mumbai, India), zinc telluride (ZnTe) (M/s Fisher Scientific, Mumbai, India), *E. coli* ATCC 25922 and Goat anti-*E. coli* antibodies were purchased from M/s Bio-Rad Labs, Gurugram, India. Anti-GAPDH (glyceraldehyde-3-phosphate dehydrogenase) monoclonal antibody and goat anti-mouse IgG secondary antibody-HRP (horse radish peroxidase) conjugate were purchased from M/s Invitrogen, Thermo Fisher Scientific, Bangalore, India, Bovine serum albumin (BSA) from M/S Sigma-Aldrich, St. Louis, MO, USA.

2.2. Methods

2.2.1. Synthesis of cadmium telluride-based (CdTe) QDs by direct aqueous synthesis

CdTe QDs were synthesized employing a direct aqueous method, using thiol stabilizer (Singh *et al.* 2016). The overall scheme for synthesis is depicted in Supplementary Figure S5.

2.2.2. Bioconjugation of QDs

2.2.2.1. Bioconjugation of QDs with Bovine serum albumin (BSA). CdTe QDs (1 mL, 31 nmol mL^{-1}) were activated by adding 25 μL of *N*′-ethylcarbodiimide hydrochloride (EDC; 400 mM in methanol) and 25 μL of *N*-hydroxysuccinimide (NHS; 100 mM in methanol) under constant stirring at room temperature (RT) for 30 min. Subsequently, the activated CdTe-MPA QDs were mixed with 10 μL of 1 and 2 mg mL^{-1} of BSA in distilled water, and allowed to react for 2 h at RT. BSA-conjugated QDs were thus separated as a pellet from the excess of free BSA by centrifugation at 5,000 rpm (4,555*g*) for 15 min. This was repeated thrice for complete removal of free BSA, and the purified BSA-conjugated QDs were stored at 4 °C, followed by a process reported previously (Donegan & Rakovich 2016; Shamsipour *et al.* 2019). The schematic flowchart in Supplementary Figure S6(a) illustrates the preparation of bioconjugation of QDs.

2.2.2.2. Bioconjugation of QDs with antibodies. CdTe-MPA QDs were activated using EDC and NHS, as described earlier. Activated QDs were mixed with 10 μg mL^{-1} of goat anti-*E. coli* antibodies in PBS (pH 7.4) and were allowed to react for 2 h at 8–10 °C. Goat anti-*E. coli*-conjugated QDs were thus separated thrice as sediment to remove excess goat anti-*E. coli* antibodies by centrifugation (5,000 rpm (4,555*g*), for 15 min) (Zhu *et al.* 2012). The purified antibody-conjugated QDs were stored at 4 °C. The schematic representation of the preparation of antibody-conjugated QDs is shown in Supplementary Figure S6(b).

2.2.3. Characterization of CdTe-MPA QDs

2.2.3.1. Determination of concentration. The concentration of CdTe QDs was determined using an ultraviolet–visible (UV–Vis) spectrophotometer (Perkin Elmer UV/VIS Spectrometer Lambda 35, Singapore). Absorption spectra were recorded and concentration of CdTe QDs was calculated employing Beer-Lambert's law (Equation (1)), as reported previously (Bunkoed & Kanatharana 2015).

$$A = \in \cdot C \cdot L \tag{1}$$

where A is the first exciton absorbance for a given sample, C is the molar concentration (mol/L) of the QDs in the sample and L is the path length (cm) of the radiation beam passing through the sample. Herein, L was fixed at 1 cm and ϵ is the extinction coefficient per mole of QDs (L/mol cm). The latter extinction coefficient (ϵ) of CdTe QDs was computed (Yu *et al.* 2003), using Equation (2).

$$\in = 3450 \cdot \Delta E \cdot (D)^{2.4} \tag{2}$$

2.2.3.2. Absorption and fluorescence spectroscopy. The optical characteristics of the synthesized CdTe-MPA QDs were explored employing UV–Vis spectroscopy and photoluminescence (PL, Hitachi F-2500 Fluorescence Spectrophotometer, Tokyo, Japan), with PL spectra recorded at an excitation wavelength of 400 nm (Tirado-Guizar *et al.* 2015).

2.2.3.3. Effect of concentration on emission intensity. PL spectroscopy was employed to study the effect of concentration on the emission intensity of QDs. Different concentrations of CdTe-MPA QDs were taken and the standard plot was made by plotting these concentrations against PL intensity.

2.2.3.4. Transmission electron microscopy (TEM). To investigate the morphology and size of the prepared CdTe-MPA QDs, TEM was carried out employing a JEOL, USA, JEM-2100 electron microscope with an acceleration voltage of 200 kV at a magnification of 230,000×. Samples were prepared for TEM analysis by depositing QDs onto the carbon-coated copper grids, followed by drying at ambient temperature. The mean of 10–20 field views of QDs was considered for recording the observations (El-Nahass *et al.* 2014).

2.2.3.5. Powder X-ray diffraction pattern (PXRD). About 10–20 mg of lyophilized CdTe-MPA QDs were subsequently analyzed at 2θ between 5° and 50° with an automated diffractometer, X'Pert PRO (M/s PAN analytical BV, Almelo, Netherlands). The radiation source was produced using Cu$K\alpha$ (PW3050/60, 1.54 Å) with an applied voltage of 45 kV, and a current of 40 mA. The overlaid diffractograms were prepared using Origin Pro 8 software (Yi & Wei 2017).

2.2.3.6. Absorption and fluorescence spectroscopy of BSA-conjugated QDs. The optical properties of BSA-conjugated CdTe-MPA QDs were investigated by UV–Vis spectroscopy and PL spectroscopy as discussed in the previous section.

2.2.3.7. Measurement of the quantum yield. The quantum yield of the hydrophilic QDs was computed using Rhodamine 6G, as per a previously reported procedure (Grabolle *et al.* 2009). Rhodamine 6G was dissolved in absolute ethanol as the reference standard (quantum yield 100%, concentration 31 nmol mL^{-1}) (Virzbickas *et al.* 2017). The relative quantum yield of the QDs was calculated using Equation (3).

$$QY_{NC} = QY_{Dye} \frac{m_{NC}}{m_{Dye}} \cdot \left(\frac{\eta_{solvent}}{\eta_{ethanol}}\right)^2 \tag{3}$$

2.2.3.8. Atomic force microscopy (AFM). Atomic force microscopy (AFM, Multimode 8, Bruker, Germany) was carried out to investigate the appearance, monodispersity and conjugation of QDs with BSA. An aliquot of 10 μL sample solution of

BSA-conjugated QDs and non-conjugated QDs each was dropped onto silicon wafers and allowed to dry for about 2 h and then subjected to analysis (Poderys *et al.* 2011).

2.2.4. Selective capturing and detection of bacteria using glass matrices

2.2.4.1. Amine functionalization of glass matrices. Glass slides were cut into square pieces (25 × 25 mm) and sonicated using acetone for 10 min in order to clean them. After drying for 10 min, these were treated with freshly prepared Piranha solution (70% H_2SO_4, 30% H_2O_2) at 55 °C for 30 min. Piranha-treated glass matrices were then again cleaned with water, methanol, methanol–toluene mixture (1:1 v/v) and toluene, under sonication for 10 min each. Silanization was then conducted by immersing these piranha-treated glass slides in 3-aminopropyl triethoxysilane solution (APTES; 2% in toluene) at RT with mild shaking for 24 h. Subsequently, for cleaning the glass slides again, these were sonicated using toluene, methanol–toluene, 1:1 (v/v) and methanol, each for 10 min, followed by baking the treated slides at 110 °C for 1 h and stored at RT (Marques *et al.* 2013). Supplementary Figure S7(a) schematically represents the piranha solution treatment, followed by silanization.

2.2.4.2. Characterization of amine-functionalized glass matrices

2.2.4.2.1. Contact angle measurements. Piranha- and silane-treated glass matrices were subjected to contact angle measurement (KRUSS drop shape analyzer) for confirmation of surface modification. A volume of 20 μL of the water drop was used for contact angle measurement. Angle (θ) formed by a drop on the surface of the matrix was recorded using a high-speed framing camera, and images processed and stored using a computer.

2.2.4.3. Evaluation of bioconjugation of antibodies with glass matrices. Bioconjugation of antibodies to the glass matrices was evaluated using an ELISA technique, employing Anti-Glyceraldehyde-3-phosphate dehydrogenase (GADPH) monoclonal primary antibody and goat anti-mouse IgH secondary antibody-conjugated with HRP. Glass matrices with functional $-NH_2$ groups were coupled with Anti-GADPH monoclonal antibody via glutaraldehyde chemistry. Anti-GADPH monoclonal antibody-conjugated glass matrices were added to microtitre plate wells, and washed in hexaplicate with PBS 7.4 to remove the free antibodies. Glass matrices were added to a 96-well plate along with 5% skimmed milk to block active sites for preventing non-specific binding. After blocking, it was washed with PBS pH 7.4, and goat anti-mouse IgH secondary antibody-conjugated with HRP was added onto glass matrices. The plate was incubated at 37 °C, once again for 2 h, followed by washing with PBS pH 7.4 (Zhu *et al.* 2012; Sahoo *et al.* 2019). These washings were then added into a 96-well plate. Substrate (100 μL, 3,3′,5, 5′-Tetramethylbenzidine) for HRP was added to each well of microtitre as well as a 96-well plate for 10 min in dark. To stop the enzyme-substrate reaction, HCl (0.1 N) as a blocking agent was added to each well to develop yellow color (Vashist *et al.* 2014). Finally, the plate was read after every 15 min and washing cycles using a micro-titre plate reader at 450 nm (Bio-Rad, Model iMark, Delhi, India).

2.2.4.4. Bioconjugation of glass matrices with goat E. coli *antibody.* Amine-functionalized glass matrices were activated with 5% glutaraldehyde for about 2 h at RT. After activation, these glass matrices were conjugated to goat *E. coli* anti-antibodies at 8–10 °C for 1 h, as schematically represented in Supplementary Figure S7(b). The conjugated glass matrices were washed thrice with PBS (pH 7.4) and stored at 2–8 °C, until used (Zhu *et al.* 2012).

*2.2.4.5. Fluorescent characteristics of goat anti-*E. coli *antibody-conjugated QDs.* The PL intensity of the goat anti-*E. coli* antibody-conjugated CdTe-MPA QDs was investigated using an excitation wavelength of 400 nm.

2.2.4.6. Gram staining. Gram staining of *E. coli* antibody-conjugated glass matrices was performed to confirm the attachment of pathogenic bacteria with an antibody. The goat *E. coli* antibody-conjugated glass matrix was washed with PBS pH 7.4, followed by the addition of the pathogenic culture of bacteria. It was kept aside for 30 min and washed again thrice with PBS pH 7.4 to remove any free bacteria. Subsequently, crystal violet, iodine, alcohol and safranin were added to the bacteria-conjugated matrix and incubated for 1 min, following each addition. The matrix was washed with running water after each addition (Beveridge 2001; Harrigan & McCance 2014) and viewed under the optical microscope (Nikon Eclipse 80i, Chiyoda-Ku, Tokyo, Japan).

2.2.4.7. Detection of pathogenic bacteria. Glass matrices-conjugated with goat anti-*E. coli* antibodies were taken, treated with *E. coli* suspension containing a varied number of bacteria (10–1,000), added onto the glass surface and incubated at 8–10 °C for 1 h, followed by washing twice with PBS, pH 7.4. A concentration of 10 μg mL^{-1} of anti-*E. coli* antibody-conjugated to the QDs containing 31 nM of CdTe-MPA QDs was selected for the detection of *E. coli* showing adequate fluorescence. Subsequently, these goat anti-*E. coli*-conjugated CdTe-MPA QDs were added to the glass matrices containing *E. coli* cells individually and incubated at 8–10 °C for 20–30 min, followed by washing twice with PBS (pH 7.4) (Figure 2; Sahoo *et al.* 2019). The bioconjugated glass matrices attached with different concentrations of *E. coli* cells as well as QDs were subjected to confocal laser scanning microscopy (CLSM) for the detection of *E. coli*. An average of 50 microscopic fields was observed on each glass matrix. Approximately, 40, 35 and 5 positive fields were discerned with glass matrices containing 1,000, 100 and 10 *E. coli* cells, respectively. Furthermore, calibration was plotted between 100, 200 and 300 no. of *E. coli* cells and PL intensity.

3. RESULTS

3.1. Synthesis of CdTe-based QDs

Figure 1 portrays the photographic image of CdTe QDs showing the fluorescent effect during various stages of the synthesis of QDs demonstrating the transition of color and intensity at a fixed excitation wavelength of 400 nm.

3.2. Characterization of CdTe-MPA QDs

3.2.1. Determination of concentration

Table 1 illustrates the spectrophotometric absorbance at the corresponding λ_{max}, band gap, particle size and the deduced concentration values of synthesized CdTe-MPA QDs.

3.2.2. Dynamic light scattering (DLS) and zeta potential measurements

The effective size as well as the size distribution of CdTe-MPA QDs, when dispersed in water, are shown in Supplementary Figure S1(a, b). The QDs exhibited relatively narrower size distribution with a mean diameter of size range 5–6 nm and a zeta potential of −31.7 mV.

3.2.3. Absorption and fluorescence spectroscopy

The CdTe QDs, stabilized with MPA, showed an absorption maximum at 360 nm (Supplementary Figure S1(c)). The CdTe-MPA QDs, on the other hand, showed prominent emission peaks at 600 nm, when excited at 400 nm (Supplementary Figure S1(d)).

Figure 1 | Photographic image of CdTe QDs showing different emission colors during synthesis.

Table 1 | Concentration and size of various synthesized CdTe-MPA QDs batches

Sample	λ_{max}	Particle size (nm)	Band Gap (eV)	Concentration (mol L^{-1})
CdTe 1	567	3.4	2.1	31.1×10^{-6}
CdTe 2	545	3.8	2.2	31.5×10^{-6}
CdTe 3	520	3.5	2.3	31.8×10^{-6}
CdTe 4	535	3.6	2.0	31.7×10^{-6}
CdTe 5	533	3.6	2.1	31.2×10^{-6}

3.2.4. Effect of concentration on emission intensity

Figure 2 shows the prominent emission peak of hydrophilic CdTe-MPA QDs at 600 nm, when excited at 400 nm. The corresponding inset represents the calibration curve between conc. of QDs and PL having linear correlation coefficient (R) as 0.9975 ($p < 0.005$).

3.2.5. Transmission electron microscopy

Figure 3 depicts the TEM images of two diverse batches of CdTe-MPA QDs, with particle size ranging between 5.4 and 6.8 nm.

3.2.6. Powder X-ray diffraction (PXRD)

Supplementary Figure S2 portrays the diffractogram pattern of the lyophilized CdTe-MPA powder, with 2θ peaks at 25°, 40° and 48° diffractions.

3.3. Characterization of BSA and antibody-conjugated CdTe QDs

Bioconjugation of water-dispersible CdTe-MPA QDs with BSA and goat anti-*E. coli* antibodies for *E. coli* detection was successfully conducted, and the following results were obtained.

3.3.1. Absorption and fluorescence spectroscopy of BSA-conjugated QDs

Absorption spectra of BSA-conjugated QDs depict a slight bump around 280 nm, as shown in Supplementary Figure S3(a). BSA-conjugated CdTe-MPA QDs demonstrated a 50–60% reduction in emission intensity at 1 mg mL^{-1} BSA concentration,

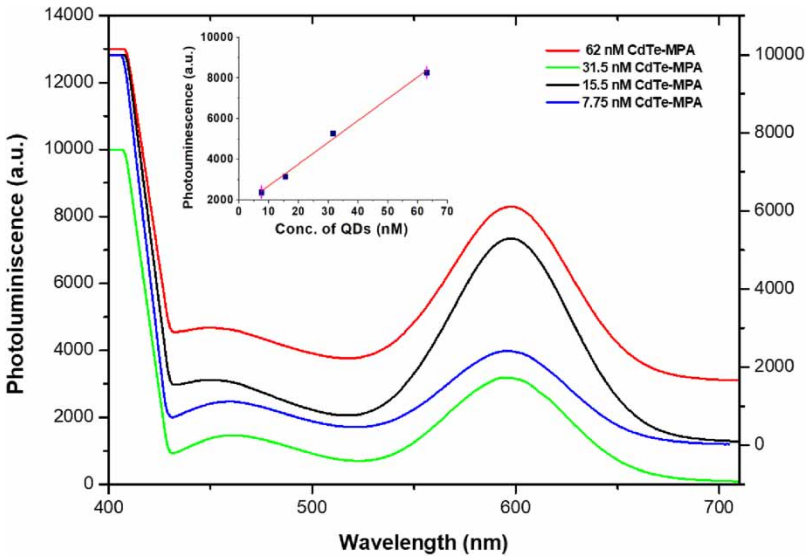

Figure 2 | Effect of concentration of quantum dots on emission spectra. The corresponding inset shows a calibration curve between conc. of QDs and photoluminescence.

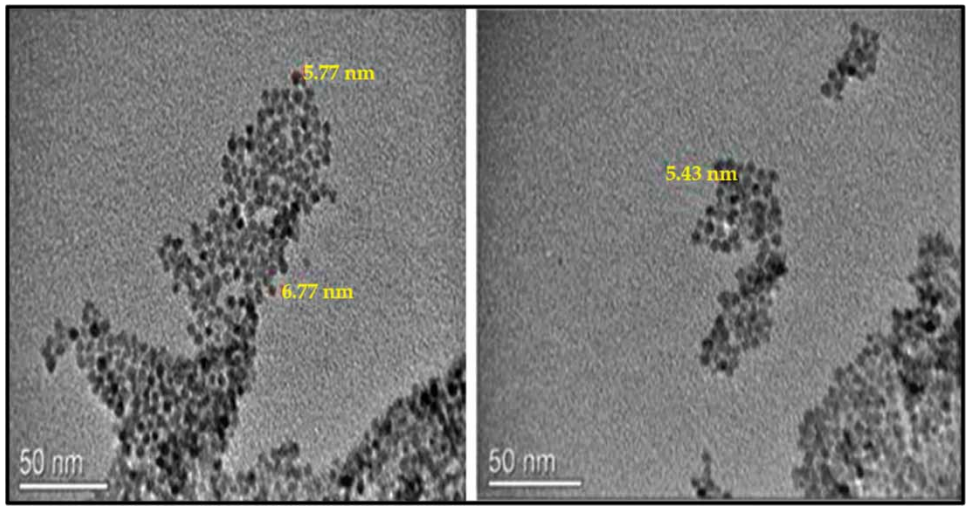

Figure 3 | TEM images of two different batches of CdTe-MPA QDs.

and a 75% reduction using a concentration of 2 mg mL^{-1}, as portrayed in Supplementary Figure S3(b). Slight bathochromic shift in peak position toward longer wavelength was observed for BSA-conjugated QDs.

3.3.2. Measurement of the quantum yield

Mean PL quantum yields of the CdTe-MPA QDs and conjugated QDs were found to be 45 ± 2% and 28 ± 5%, respectively.

3.3.3. Fourier-transform infrared spectroscopy (FTIR)

The FTIR spectra in Supplementary Figure S4(a, b) depict carbonyl group stretching vibration at 1,690.32 cm^{-1} in naïve QDs to peaks 1,638.91 and 1,637.80 cm^{-1} in BSA-conjugated QDs.

3.3.4. Atomic force microscopy (AFM)

Supplementary Figure S1(e) (i, ii, iii) portrays the AFM images of non-conjugated and BSA-conjugated CdTe-MPA QDs, respectively. Supplementary Table S1 shows the root-mean-square roughness (R_q) and mean roughness (R_a) values of 1.603 and 1.273, and of 0.565 and 0.386 for BSA-conjugated QDs, respectively.

3.4. Selective capturing and detection of bacteria using glass matrices

3.4.1. Characterization of amine-functionalized glass matrices

3.4.1.1. Contact angle measurements. Figure 4 shows the contact angle (θ) values of the water droplets as observed on various glass surfaces. The values of θ on the glass surface, after piranha solution treatment and silane functionalization, are enlisted in Table 2 indicating enhancement in water contact angle.

3.4.2. Evaluation of bioconjugation of antibodies with glass matrices

Figure 5 shows the absorbance values of GAPDH monoclonal antibody-conjugated glass matrices and washings.

3.4.3. Fluorescent properties of antibody-conjugated QDs

Figure 6 depicts the emission spectra of the non-conjugated and goat anti-*E. coli* antibody-conjugated CdTe-MPA QDs with a prominent emission peak at 600 and 610 nm, respectively, after excitation at 400 nm.

3.4.4. Gram staining

Figure 7 exhibits pink-colored optical microscopic images of the glass slides, incubated with antibody-attached *E. coli*, on treatment with different chemicals.

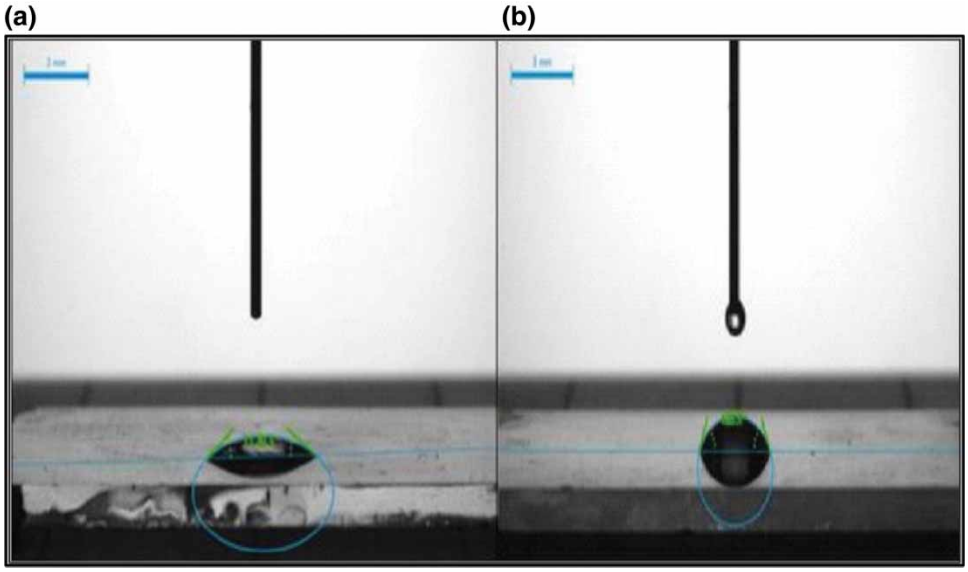

Figure 4 | Water contact angle (θ) on the surface of (a) piranha solution-treated glass matrix and (b) silane-functionalized glass matrix.

Table 2 | Water contact angle (θ) measurement of the glass matrix

S No	Glass matrix	Contact angle (°) mean ± SD
1	Piranha solution-treated glass matrix	30.65 ± 0.63
2	Silane-functionalized glass matrix	67.45 ± 2.95

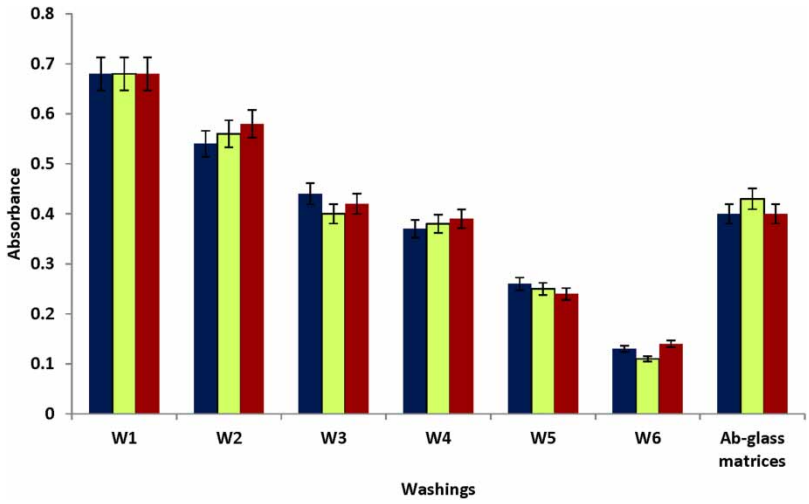

Figure 5 | Values of optical density observed during ELISA for confirming bioconjugation of GADPH monoclonal antibody to amine-functionalized glass matrices. The cross-bars indicate ± 1 SD.

3.4.5. Detection of pathogenic bacteria

Intense yellow fluorescence was observed, when antibody-conjugated glass matrices containing *E. coli* cells were incubated with anti-*E. coli* antibody-conjugated QDs. Likewise, the glass matrices, when incubated with 10, 100 and 1,000 cells, showed

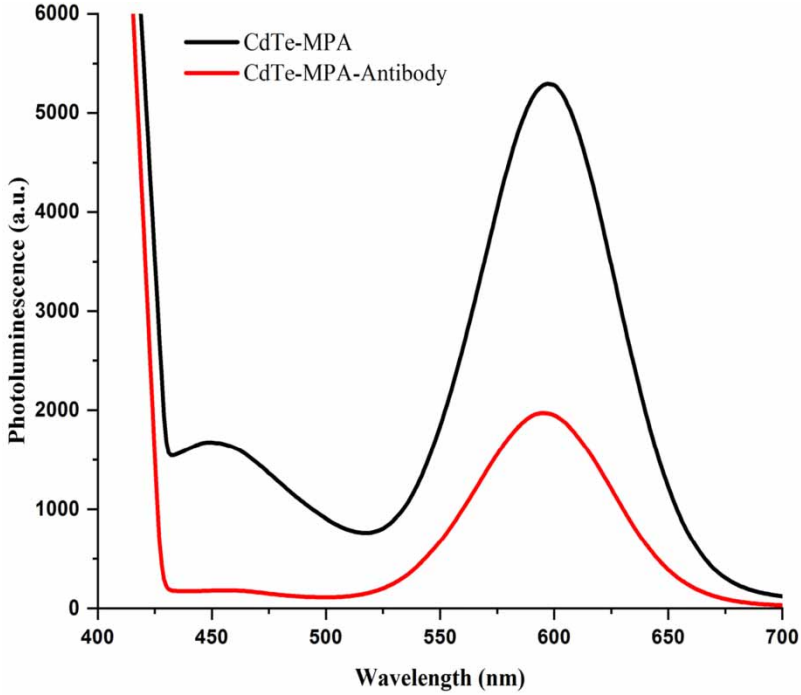

Figure 6 | Photoluminescence spectra of non-conjugated and anti-*E. coli* antibody-conjugated CdTe-MPA QDs.

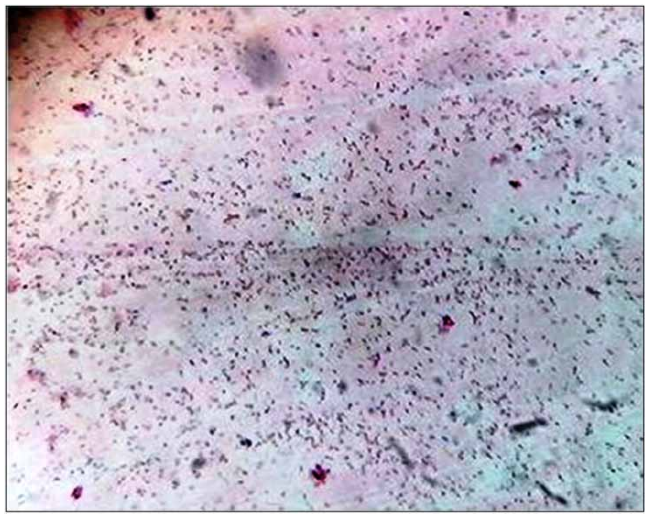

Figure 7 | Glass slides incubated with antibody-attached *E. coli*, as observed under the optical microscope.

intense yellow-colored fluorescence under the CLSM field (Figure 8). The corresponding inset represents the calibration curve between no. of bacterial cells and PL having linear correlation coefficient (R) as 0.998.

4. DISCUSSION

Table 1 enumerates the values of λ_{max} values of the synthesized QDs, ranging between 533 and 567 nm, band gap between 2.0 and 2.3 eV, and concentration between 31.1 and 31.8 μmol/L (Table 1), indicating the reproducibility and robustness of the synthesis protocol of QDs during our work. On increasing the reflux time during the synthesis, the fluorescence color of CdTe QDs under UV irradiation changed from green to red, i.e., toward higher wavelengths (Figure 1), ostensibly due to increased

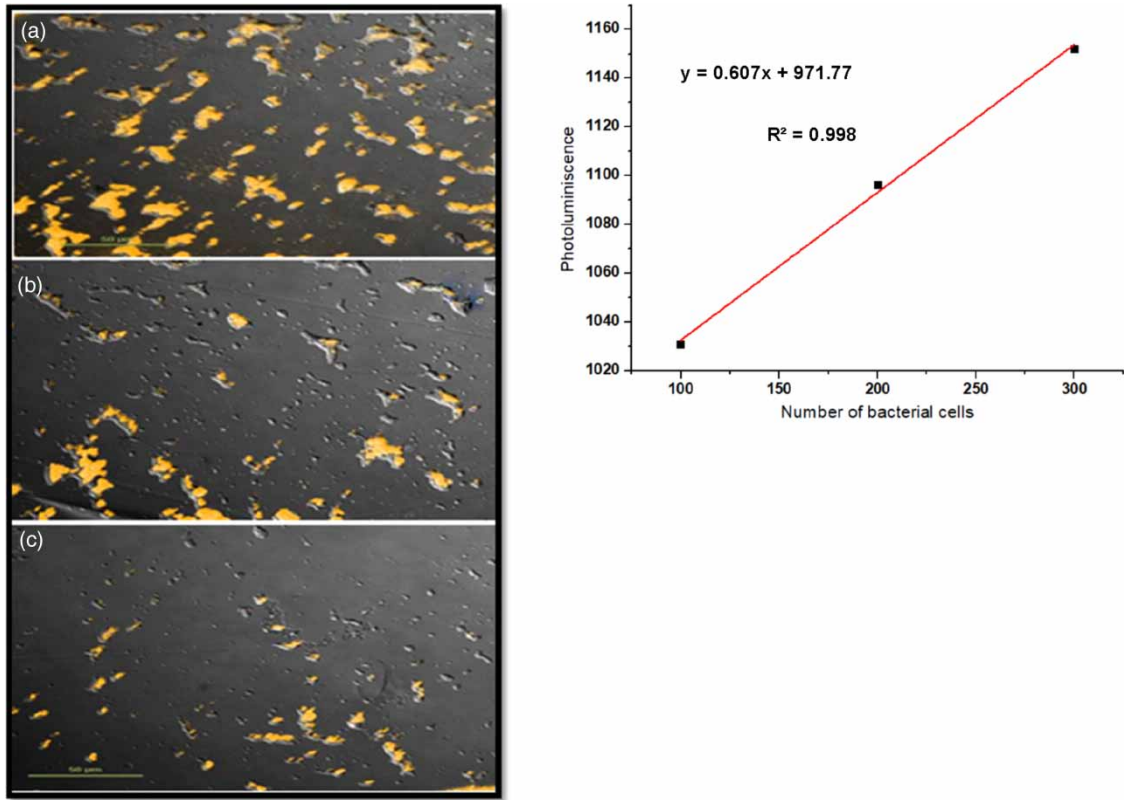

Figure 8 | Confocal laser microscopic images detected with anti-*E. coli* antibody-conjugated CdTe QDs captured on functionalized glass matrices with (a) 1,000, (b) 100 and (c) 10 *E. coli* cells. The corresponding inset shows a calibration curve between no. of bacterial cells and photoluminescence.

size of QDs, as a consequence of reduced quantum confinement (Smith *et al.* 2009; Liu *et al.* 2010; Shen *et al.* 2013). It was therefore deduced that the size of CdTe QDs is directly proportional to the emission fluorescence wavelength, which could be controlled by the reflux duration. The colloidal stability and particle size, as measured using the DLS study (Supplementary Figure S1(a, b)), depicted that the CdTe-MPA QDs were formed with a narrow size distribution and high magnitude of zeta potential, i.e., −31.7 mV, indicating the potential robustness of QDs owing to strong repulsive forces, thus preventing any possible aggregation of NPs (Kalangi *et al.* 2018; Li *et al.* 2020). The size distribution and stability were further confirmed using TEM analysis too (Figure 3), delineating the formation of monodispersed spherical-shaped QDs (Wang & Qiu 2016). The emission spectrum of CdTe-MPA QDs (Supplementary Figure S1(c)) exhibited quite symmetrical and narrow spectral width (Supplementary Figure S1(d)), indicating adequate spectral resolution for the quantitative detection of the fluorescence intensity. Increasing the concentration of QDs caused a significant rise in the emission intensity (Figure 2), with hardly any shift in emission wavelength. This can be assigned to the uniform dispersion of QDs in PBS (pH 7.4) and non-interference of ligands attached to the surface of QDs (Singh *et al.* 2011). The diffractogram of QDs (Figure 8) showed a broad peak at $2\theta = 25°$, attributable to the nanocrystalline nature of MPA-capped CdTe QDs, in consonance with previous literature (Ung *et al.* 2012).

BSA was selected for bioconjugation, as a high molecular weight protein possesses physicochemical properties quite analogous to that of the antibodies, which are to be ultimately employed during further studies (Singh *et al.* 2014). Successful bioconjugation of proteins and antibodies to carboxylated CdTe QDs could be rationally attributed to EDC, the most commonly used zero-length cross-linker, on account of its high efficiency and resultant high yield of bioconjugate formation in a controlled manner (Grabarek & Gergely 1990).

A concentration-dependent reduction in the fluorescent intensity of QDs was noticeable on bioconjugation with BSA, ascribable to the possible change in the electronic energy of QDs, owing to interactions of these ligands with the surface of QDs (Singh *et al.* 2015). The modified QDs, nevertheless, were found to retain substantial fluorescent properties

(Supplementary Figure S3(a, b)). Furthermore, the mean quantum yield of conjugated QDs relative to that of non-conjugated ones was about 62%, suggesting substantial retention in the fluorescent characteristics of the QDs, even after bioconjugation (Ferrari & Bergquist 2007; Virzbickas *et al.* 2017).

The FTIR spectroscopy (Supplementary Figure S4(a, b)) was employed to investigate the optical properties of QDs, it being a versatile technique for identification and characterization of various functional groups present on the surface of QDs (Fine *et al.* 2020). The presence of BSA around CdTe-MPA QDs can be deciphered by the existence of all the main signals, with almost similar C = O stretching vibration of the carbonyl groups at 1,638.91 and 1,637.80 cm^{-1} (Singh *et al.* 2011). Such results formed the basis for further bioconjugation studies with goat anti-*E. coli* antibodies. Also, the AFM images of BSA-conjugated QDs, with R_q and R_a values of 0.565 and 0.386, respectively (Supplementary Figure S1(e) and Table S1), construed smoothness of the BSA-conjugated QDs and their potential stability, after bioconjugation with ligands (Abha *et al.* 2020).

Subjecting antibody-bioconjugation to EDC/NHS activation resulted in the formation of highly reactive intermediate, i.e., NHS-carboxylate, and desired nanoconjugates of the antibody with CdTe-MPA QDs (Tripathi *et al.* 2016). The fluorescent nature of the non-conjugated QDs and goat anti-*E. coli* antibody-conjugated QDs (Figure 6) depict a fourfold reduction in the emission intensity with minuscule bathochromic shift, i.e., peak position shifting toward longer wavelength. The aforesaid properties of QDs vividly indicate the presence of antibody on the surface of QDs and their vast promise as efficient fluorescent signal-producing tools for detecting microorganisms, like *E. coli*. Hence, successful bioconjugation of anti-*E. coli* antibodies with QDs was corroborated by the decline in their emission intensity vis-à-vis that of the unconjugated CdTe-MPA QDs, delineating the presence of antibody on the surface of QDs.

Since QDs need a suitable platform to efficiently capture the bacteria and assist in their detection, the glass matrices were employed for the purpose. Such glass matrices are documented to be hydrophobic, optically transparent and effective for selective capturing of pathogens after apt chemical or biological modification (Renuka *et al.* 2018). Hence, these were further surface-functionalized with amine groups using piranha solution with θ value of 30.65 ($\pm$0.63), as the generation of hydroxyl groups on the outer surface area of glass matrix resulted in more hydrophilic characteristics (Marques *et al.* 2013). Accordingly, the functionalized glass matrix was silanized (Supplementary Figure S7(a)), resulting in the augmentation of hydrophobicity and water contact angle of 67.45 $\pm$ 2.95 (Table 2), thus enabling feasible antibody conjugation. On the basis of the absorbance values of GADPH monoclonal antibody-conjugated glass matrices, determined periodically after every 15 min, and washing cycles (Figure 5) using the ELISA technique, an optimum incubation time of 2 h was selected indicating the efficiency of glass matrices for bioconjugation with the antibody (Tripathi *et al.* 2016; Chandan *et al.* 2018). After these successive washings and 2 h of incubation time, the absorbance of these functionalized glass matrices (10 $\mu g\ mL^{-1}$ GADPH monoclonal antibody) tended to decrease due to the removal of free (i.e., unconjugated) antibodies. Lastly, a high absorbance value (i.e., 0.41) was observed signifying the complete removal of free antibodies and their potential for further bioconjugation with *E. coli*-specific antibody(ies).

Bioconjugation of anti-*E. coli* antibodies with glass matrices was accomplished by the formation of covalent bond via glutaraldehyde chemistry (Renuka *et al.* 2018; Supplementary Figure S7(a)). Gram staining using safranin clearly indicated the presence of pink color (Figure 7), ostensibly owing to the existence of a thick mesh-like cell wall, made up of peptidoglycan (50–90% of cell envelope) for a Gram-negative bacterium, i.e., *E. coli* (Beveridge 2001). This antigen/antibody interaction on glass matrices rendered selective capturing of *E. coli* cells by antibody-conjugated glass matrices, thus paving a way for developing a fluorescent-based detection probe employing QDs (Bhardwaj *et al.* 2017). The presence of yellow-colored fluorescence, observed during CLSM imaging (Figure 8), confirmed the attachment of *E. coli* antibody-conjugated glass matrices containing 1,000, 100 and 10 *E. coli* cells and CdTe-MPA QDs conjugated with anti-*E. coli* antibody. The calibration curve between no. of bacterial cells and PL illustrated a linear correlation coefficient (R) as 0.998 indicating effective capturing of 100, 200 and 300 *E. coli* cells, respectively, by the anti-*E. coli* antibody-conjugated QDs.

Overall, the CdTe QDs, synthesized using MPA-a thiol stabilizer, exhibited improved optical properties, aqueous dispersibility and uniform particle size. It may be ascribed to the tendency of the thiol molecule to firmly stick to the surface of the resultant QDs via Cd–SH bonds, thus preventing the uncontrollable nuclei growth (Li *et al.* 2011; Kaczmarek *et al.* 2016). Hence, this sandwich model corroborated the utility of CdTe-MPA QDs for the successful detection of *E. coli* cells, i.e., 10 organisms/mL, demonstrating high sensitivity and specificity of the developed fluorescent probe.

5. CONCLUSION

The current research work reports the successful development of fluorescent bioconjugated-QDs for efficient detection of *E. coli* ATCC 25922. Synthesized using the direct aqueous method and subsequently conjugated with anti-*E. coli* antibodies, the CdTe-MPA QDs were found to be monodispersed and spherically shaped. The high quantum yield of conjugated CdTe-MPA QDs with significant fluorescent characteristics ratified their utility as an effective microbial detection tool. Bioconjugation of goat anti-*E. coli* antibodies with glass matrices, as well as QDs, studied using ELISA and CLSM, demonstrated selective detection of *E. coli*. In a nutshell, the silane-functionalized glass matrices and cadmium-based QDs hold considerable potential for efficient detection of *E. coli* in water samples, without any interference with the complexity and interaction(s) of other bacterial species, unless they are specifically surface-modified using antigen–antibody interaction(s). The aforementioned technology can further be rationally extended and explored for the detection of other pathogenic microorganisms in myriad samples too.

ACKNOWLEDGEMENTS

The authors gratefully acknowledge the financial grants received from DST-UT (19-20)/Sanc/10/2019/1703-1710, dated 31.10.2019), Government of India. R.P.B. and G.S. appreciate the support granted by UGC, New Delhi, India, under Faculty Recharge Program.

DATA AVAILABILITY STATEMENT

All relevant data are included in the paper or its Supplementary Information.

CONFLICT OF INTEREST

The authors declare there is no conflict.

REFERENCES

Abha, K., Sumithra, I., Suji, S., Anjana, R., Devi, J. A., Nebu, J., Lekha, G., Aparna, R. & George, S. 2020 Dopamine-induced photoluminescence quenching of bovine serum albumin-capped manganese-doped zinc sulphide quantum dots. *Analytical and Bioanalytical Chemistry* **412** (23), 5671–5681.

Acharya, G., Mitra, A. K. & Cholkar, K. 2017 Nanosystems for diagnostic imaging, biodetectors, and biosensors. In: *Emerging Nanotechnologies for Diagnostics, Drug Delivery and Medical Devices*. (Cholkar, K., Mitra, A.K., Mandal, A., eds.) Elsevier, Amsterdam, pp. 217–248.

Alahi, M. E. E. & Mukhopadhyay, S. C. 2017 Detection methodologies for pathogen and toxins: a review. *Sensors* **17** (8), 1885.

Bedi, N., Srivastava, D. K., Srivastava, A., Mahapatra, S., Dkhar, D. S., Chandra, P. & Srivastava, A. 2022 Marine biological macromolecules as matrix material for biosensor fabrication. *Biotechnology and Bioengineering* **119** (8), 2046–2063.

Beveridge, T. J. 2001 Use of the Gram stain in microbiology. *Biotechnic & Histochemistry* **76** (3), 111–118.

Bhardwaj, N., Bhardwaj, S. K., Nayak, M. K., Mehta, J., Kim, K.-H. & Deep, A. 2017 Fluorescent nanobiosensors for the targeted detection of foodborne bacteria. *Trends in Analytical Chemistry* **97**, 120–135.

Bhardwaj, N., Bhardwaj, S. K., Bhatt, D., Lim, D. K., Kim, K.-H. & Deep, A. 2019 Optical detection of waterborne pathogens using nanomaterials. *Trends in Analytical Chemistry* **113**, 280–300.

Bunkoed, O. & Kanatharana, P. 2015 Mercaptopropionic acid-capped CdTe quantum dots as fluorescence probe for the determination of salicylic acid in pharmaceutical products. *Luminescence* **30** (7), 1083–1089.

Bursle, E. & Robson, J. 2016 Non-culture methods for detecting infection. *Australian Prescriber* **39** (5), 171–175.

Chandan, H. R., Schiffman, J. D. & Balakrishna, R. G. 2018 Quantum dots as fluorescent probes: synthesis, surface chemistry, energy transfer mechanisms, and applications. *Sensors and Actuators B: Chemical* **258**, 1191–1214.

Donegan, J. & Rakovich, Y. 2016 *Cadmium Telluride Quantum Dots: Advances and Applications*. Jenny Stanford Publishing, Boca Raton, FL.

Du, H., Wang, X., Yang, Q. & Wu, W. 2021 Quantum dot: lightning invisible foodborne pathogens. *Trends in Food Science and Technology* **110**, 1–12.

El-Nahass, M., Youssef, G. & Noby, S. Z. 2014 Structural and optical characterization of CdTe quantum dots thin films. *Journal of Alloys and Compounds* **604**, 253–259.

Ferrari, B. & Bergquist, P. 2007 Quantum dots as alternatives to organic fluorophores for Cryptosporidium detection using conventional flow cytometry and specific monoclonal antibodies: lessons learned. *Cytometry Part A: The Journal of the International Society for Analytical Cytology* **71** (4), 265–271.

Fine, J. A., Rajasekar, A. A., Jethava, K. P. & Chopra, G. 2020 Spectral deep learning for prediction and prospective validation of functional groups. *Chemical Science* **11** (18), 4618–4630.

Grabarek, Z. & Gergely, J. 1990 Zero-length crosslinking procedure with the use of active esters. *Analytical Biochemistry* **185** (1), 131–135.

Grabolle, M., Spieles, M., Lesnyak, V., Gaponik, N., Eychmüller, A. & Resch-Genger, U. 2009 Determination of the fluorescence quantum yield of quantum dots: suitable procedures and achievable uncertainties. *Analytical Chemistry* **81** (15), 6285–6294.

Harrigan, W. F. & McCance, M. E. 2014 *Laboratory Methods in Microbiology*. Academic Press, London.

Kaczmarek, H., Metzler, M. & Węgrzynowska-Drzymalska, K. 2016 Effect of stabilizer type on the physicochemical properties of poly (acrylic acid)/silver nanocomposites for biomedical applications. *Polymer Bulletin* **73** (10), 2927–2945.

Kalangi, S. K., Swarnakar, N. K., Sathyavathi, R., Narayana Rao, D., Jain, S. & Reddanna, P. 2018 Synthesis, characterization, and biodistribution of quantum dot-celecoxib conjugate in mouse paw edema model. *Oxidative Medicine and Cellular Longevity* **2018**, 1–8.

Kuzyniak, W., Adegoke, O., Sekhosana, K., D'Souza, S., Tshangana, S. C., Hoffmann, B., Ermilov, E. A., Nyokong, T. & Höpfner, M. 2014 Synthesis and characterization of quantum dots designed for biomedical use. *International Journal of Pharmaceutics* **466** (1–2), 382–389.

Law, J. W.-F., Ab Mutalib, N.-S., Chan, K.-G. & Lee, L.-H. 2015 Rapid methods for the detection of foodborne bacterial pathogens: principles, applications, advantages and limitations. *Frontiers in Microbiology* **5**, 770.

Lee, J.-H., Kim, H. H., Cho, Y. H., Koo, T.-S. & Lee, G. W. 2018 Development and evaluation of raloxifene hydrochloride-loaded supersaturatable SMEDDS containing an acidifier. *Pharmaceutics* **10** (3), 78.

Li, Z., Dong, C., Tang, L., Zhu, X., Chen, H. & Ren, J. 2011 Aqueous synthesis of CdTe/CdS/ZnS quantum dots and their optical and chemical properties. *Luminescence* **26** (6), 439–448.

Li, C., Hassan, A., Palmai, M., Snee, P. T., Baveye, P. C. & Darnault, C. J. 2020 Colloidal stability and aggregation kinetics of nanocrystal CdSe/ZnS quantum dots in aqueous systems: effects of pH and organic ligands. *Journal of Nanoparticle Research* **22** (11), 1–29.

Li, D., Liu, L., Huang, Q., Tong, T., Zhou, Y., Li, Z., Bai, Q., Liang, H. & Chen, L. 2021 Recent advances on aptamer-based biosensors for detection of pathogenic bacteria. *World Journal of Microbiology and Biotechnology* **37** (3), 1–20.

Liu, Y., Miyoshi, H. & Nakamura, M. 2007 Nanomedicine for drug delivery and imaging: a promising avenue for cancer therapy and diagnosis using targeted functional nanoparticles. *International Journal of Cancer* **120** (12), 2527–2537.

Liu, J., Shi, Z., Yu, Y., Yang, R. & Zuo, S. 2010 Water-soluble multicolored fluorescent CdTe quantum dots: synthesis and application for fingerprint developing. *Journal of Colloid and Interface Science* **342** (2), 278–282.

Luo, K., Kim, H.-Y., Oh, M.-H. & Kim, Y.-R. 2020 Based lateral flow strip assay for the detection of foodborne pathogens: principles, applications, technological challenges and opportunities. *Critical Review Food Science and Nutrition* **60** (1), 157–170.

Mansuriya, B. D. & Altintas, Z. 2020 Applications of graphene quantum dots in biomedical sensors. *Sensors* **20** (4), 1072.

Marques, M. E., Mansur, A. A. & Mansur, H. S. 2013 Chemical functionalization of surfaces for building three-dimensional engineered biosensors. *Applied Surface Science* **275**, 347–360.

Nie, S., Xing, Y., Kim, G. J. & Simons, J. W. 2007 Nanotechnology applications in cancer. *Annual Review of Biomedical Engineering* **9**, 257–288.

Pandit, C., Alajangi, H. K., Singh, J., Khajuria, A., Sharma, A., Hassan, M. S., Parida, M., Semwal, A. D., Gopalan, N., Sharma, R. K., Suttee, A., Soni, U., Singh, B., Sapra, S., Barnwal, R. P., Singh, G. & Kaur, I. P. 2022 Development of magnetic nanoparticle assisted aptamer-quantum dot based biosensor for the detection of *Escherichia coli* in water samples. *Science of The Total Environment* **831**, 154857.

Pang, B., Zhao, C., Li, L., Song, X., Xu, K., Wang, J., Liu, Y., Fu, K., Bao, H. & Song, D. 2018 Development of a low-cost paper-based ELISA method for rapid *Escherichia coli* O157: H7 detection. *Analytical Biochemistry* **542**, 58–62.

Petronella, F., De Biase, D., Zaccagnini, F., Verrina, V., Lim, S.-I., Jeong, K.-U., Miglietta, S., Petrozza, V., Scognamiglio, V. & Godman, N. P. 2022 Label-free and reusable antibody-functionalized gold nanorod arrays for the rapid detection of *Escherichia coli* cells in a water dispersion. *Environmental Science: Nano* **9** (9), 3343–3360.

Poderys, V., Matulionyte, M., Selskis, A. & Rotomskis, R. 2011 Interaction of water-soluble CdTe quantum dots with bovine serum albumin. *Nanoscale Research Letters* **6** (1), 9.

Ravikumar, C. H., Shwetharani, R. & Balakrishna, R. G. 2020 Surface modified glass substrate for sensing *E. coli* using highly stable and luminescent CdSe/CdS core shell quantum dots. *Journal of Photochemistry and Photobiology B: Biology* **204**, 111799.

Renuka, R., Achuth, J., Chandan, H., Venkataramana, M. & Kadirvelu, K. 2018 A fluorescent dual aptasensor for the rapid and sensitive onsite detection of *E. coli* O157: H7 and its validation in various food matrices. *New Journal of Chemistry* **42** (13), 10807–10817.

Sahoo, S. L., Liu, C.-H., Kumari, M., Wu, W.-C. & Wang, C.-C. 2019 Biocompatible quantum dot-antibody conjugate for cell imaging, targeting and fluorometric immunoassay: crosslinking, characterization and applications. *RSC Advances* **9** (56), 32791–32803.

Shamsipour, M., Mansouri, A. M. & Moradipour, P. 2019 Temozolomide conjugated carbon quantum dots embedded in core/shell nanofibers prepared by coaxial electrospinning as an implantable delivery system for cell imaging and sustained drug release. *AAPS PharmSciTech* **20** (7), 1–14.

Shen, M., Jia, W., You, Y., Hu, Y., Li, F., Tian, S., Li, J., Jin, Y. & Han, D. 2013 Luminescent properties of CdTe quantum dots synthesized using 3-mercaptopropionic acid reduction of tellurium dioxide directly. *Nanoscale Research Letters* **8** (1), 1–6.

Singh, G., Zaidi, N. H., Soni, U., Gautam, M., Jackeray, R., Singh, H. & Sapra, S. 2011 Detection of bioconjugated quantum dots passivated with different ligands for bio-applications. *Journal of Nanoscience and Nanotechnology* **11** (5), 3834–3842.

Singh, A., Chaudhary, S., Agarwal, A., Verma, A. S., 2014 Antibodies: monoclonal and polyclonal. In: *Animal Biotechnology* (Verma, A. S. & Singh, A., eds). Academic Press, San Diego, pp. 265–287.

Singh, G., Kumar, M., Soni, U., Arora, V., Bansal, V., Gupta, D., Bhat, M., Dinda, A. K., Sapra, S. & Singh, H. 2015 Cancer cell targeting using folic acid/anti-HER2 antibody conjugated fluorescent CdSe/CdS/ZnS-MPA and CdTe-MSA quantum dots. *Journal of Nanoscience and Nanotechnology* **15** (12), 9382–9395.

Singh, G., Kumar, M., Soni, U., Arora, V., Bansal, V., Gupta, D., Bhat, M., Dinda, A. K., Sapra, S. & Singh, H. 2016 Cancer cell targeting using folic acid/anti-HER2 antibody conjugated fluorescent CdSe/CdS/ZnS-Mercaptopropionic acid and CdTe-Mercaptosuccinic acid quantum dots. *Journal of Nanoscience and Nanotechnology* **16** (1), 130–143.

Singh, G., Singh, B., Kaur, I. & Suttee, A. 2020 Selective capturing and detection of pathogens on glass matrix using affinity moiety coupled quantum dots. *Indian Patent, India*. Application number 201911005835 A.

Smith, A. M., Mohs, A. M. & Nie, S. 2009 Tuning the optical and electronic properties of colloidal nanocrystals by lattice strain. *Nature Nanotechnology* **4** (1), 56–63.

Tirado-Guizar, A., Pina-Luis, G. & Paraguay-Delgado, F. 2015 Fluorescence enhancement study of shell-less CdTe quantum dots. *Materials Express* **5** (1), 33–40.

Tripathi, S. K., Khurana, R. K., Kaur, G. & Singh, B. 2016 Quantum dots: dynamic tools in cancer nanomedicine. In: *Nanobiomaterials in Medical Imaging*. (Grumezescu, A.M., ed.) Elsevier, Amsterdam, pp. 71–100.

Ung, T. D. T., Tran, T. K. C., Pham, T. N., Nguyen, D. N., Dinh, D. K. & Nguyen, Q. L. 2012 CdTe and CdSe quantum dots: synthesis, characterizations and applications in agriculture. *Advances in Natural Sciences: Nanoscience and Nanotechnology* **3** (4), 043001.

Vashist, S. K., Schneider, E. M., Lam, E., Hrapovic, S. & Luong, J. H. 2014 One-step antibody immobilization-based rapid and highly-sensitive sandwich ELISA procedure for potential in vitro diagnostics. *Scientific Reports* **4**, 4407.

Virzbickas, K., Rimkute, L., Harvie, A. J. & Critchley, K. 2017 Surfactant-dependent photoluminescence of CdTe/CdS nanocrystals. *Journal of Experimental Nanoscience* **12** (1), 94–103.

Wang, J. & Qiu, J. 2016 A review of carbon dots in biological applications. *Journal of Materials Science* **51** (10), 4728–4738.

Wu, L., Li, G., Xu, X., Zhu, L., Huang, R. & Chen, X. 2019 Application of nano-ELISA in food analysis: recent advances and challenges. *Trends in Analytical Chemistry* **113**, 140–156.

Yi, K.-Y. & Wei, C.-S. 2017 Electrochemiluminescence of CdTe quantum dots and sensitive detection of hemoglobin. *International Journal of Electrochemical Science* **12** (4), 3472–3482.

Yu, W. W., Qu, L., Guo, W. & Peng, X. 2003 Experimental determination of the extinction coefficient of CdTe, CdSe, and CdS nanocrystals. *Chemistry of Materials* **15** (14), 2854–2860.

Zhang, Y., Zhu, L., He, P., Zi, F., Hu, X. & Wang, Q. 2019 Sensitive assay of *Escherichia coli* in food samples by microchip capillary electrophoresis based on specific aptamer binding strategy. *Talanta* **197**, 284–290.

Zhu, H., Sikora, U. & Ozcan, A. 2012 Quantum dot enabled detection of *Escherichia coli* using a cell-phone. *Analyst* **137** (11), 2541–2544.

First received 14 November 2021; accepted in revised form 12 November 2022. Available online 21 November 2022